Transition Aero-Propulsive Analysis of a Tilt-Wing eVTOL Aircraft Using a Surface-Vorticity Solver

Griffin A. DiMaggio*
Department of Aerospace Engineering, Auburn University, Auburn, Alabama 36832

Benjamin M. Simmons† and Steven C. Geuther‡
NASA Langley Research Center, Hampton, Virginia 23681

Roy J. Hartfield Jr.§
Department of Aerospace Engineering, Auburn University, Auburn, Alabama 36832

Vivek Ahuja¶
Altair Engineering, Troy, Michigan 48083

This work uses FlightStream®, a surface-vorticity solver, to perform an aero-propulsive analysis on the NASA LA-8 aircraft through the transition flight regime. Aerodynamic force and moment coefficient predictions for forward and transition flight of the airframe without propulsors are compared with wind tunnel data. Powered transition cases are simulated using Conway actuator disks to model the propellers and results are compared with response surface equations derived from wind tunnel data. The approach described in the paper provides mid-fidelity solutions at a reduced computational cost compared to volumetric CFD, which allows for rapid transition flight analyses and optimization in the early design stages. The best prediction results were observed in forward flight and high-speed transition. Mid-transition results were not as close in magnitude, but the trends exhibited reasonable agreement with experimental data.

Nomenclature

b	=	wingspan, ft
C_D	=	drag coefficient
C_L	=	lift coefficient
C_T	=	thrust coefficient
C_l	=	rolling moment coefficient
C_m	=	pitching moment coefficient
c_{ref}	=	reference chord, ft
$c_{0.75}$	=	blade chord at 75% blade length, ft
D	=	propeller diameter, ft
i_p	=	propeller incidence angle, deg
J_x	=	normal advance ratio component
J_z	=	edgewise advance ratio component
$\bar{q}$	=	dynamic pressure, psf
n	=	propeller rotational speed, rpm
R	=	propeller radius, ft
Re	=	Reynolds number
S_{ref}	=	reference area, ft^2

*Research Assistant, Department of Aerospace Engineering, AIAA Student Member.
†Research Aerospace Engineer, Flight Dynamics Branch, Member AIAA.
‡Aerospace Engineer, Aeronautics Systems Engineering Branch.
§Woltosz Professor, Department of Aerospace Engineering, Associate Fellow.
¶Director of FlightStream® Products, Altair Engineering, AIAA Senior Member.

T = thrust, lbf
V_∞ = freestream velocity, ft/s
α = angle of attack, deg
β = sideslip angle, deg
δ_e = elevon deflection angle, deg
δ_w = wing angle, deg
μ = viscosity, lbf-s/ft^2
ρ = air density, slug/ft^3

I. Introduction

Recent Advanced Air Mobility (AAM) initiatives have encouraged the development of diverse classes of distributed electric propulsion (DEP) aircraft with configurations enabling electric vertical takeoff and landing (eVTOL), electric short takeoff and landing (eSTOL), and electric conventional takeoff and landing (eCTOL) [1–4]. AAM encompasses Urban Air Mobility (UAM) that pertains to efficient air travel and cargo delivery in urban environments and Regional Air Mobility (RAM) that focuses on similar rural applications. The AAM field must overcome many technical challenges before the industry can reach maturity; these include airworthiness certification, air traffic management, pilot-operator interface, handling qualities, simplified vehicle operations, contingency management, vehicle autonomy, and flight control strategies [5]. Additionally, designing these aircraft poses its challenges [6, 7].

The unconventional geometry of aircraft supporting AAM missions often does not have any past legacy data to help base design decisions, which results in the need for rigorous testing and/or simulation. Moreover, the proprietary nature of current eVTOL aircraft research and development makes it challenging to validate computational tools that could assist development. Hover, transition, and forward flight regimes, all with high aero-propulsive coupling from the DEP system, need to be investigated and characterized. Furthermore, these vehicles typically have a large number of control effectors with varying effectiveness over the full flight envelope that need to be understood. Experimental investigation can be costly and time-consuming, especially in early stages of design. Computational fluid dynamics (CFD) is generally too expensive, both in terms of computation time and mesh preparation, to perform sufficient transition flight analyses in early design stages, particularly when the aircraft geometry changes during transition. Meshing is considered a primary bottleneck in the CFD workflow [8]. This work uses FlightStream®, a surface-vorticity solver developed by Research in Flight, to perform an efficient aerodynamic analysis suitable for preliminary design of an eVTOL aircraft with particular focus on the transition flight corridor. At its core, FlightStream® is a potential flow solver; however, the inclusion of integral boundary layer models, a viscous-coupling technique, and a surface-based flow separation correction [9, 10] allow it to produce solutions with a fidelity comparable to Reynolds-averaged Navier-Stokes (RANS) CFD, at a fraction of computational cost [11, 12]. FlightStream®'s efficiency primarily stems from the fact that only a surface mesh is required for the computational model as opposed to the volumetric mesh used in traditional CFD.

To help investigate eVTOL aircraft, NASA Langley Research Center conducted wind tunnel and flight tests on a series of subscale testbed aircraft, which resulted in a better understanding of the transition corridor and the effects of DEP [13–15]. These efforts were partly conducted to provide accessible eVTOL geometry and experimental data to validate computational tools and develop new design techniques [16]. The vehicle used for this work was the Langley Aerodrome No. 8 (LA-8), a tandem tilt-wing eVTOL aircraft [14]. Extensive one-factor-at-a-time wind tunnel tests were conducted for the LA-8 where data were collected for unpowered and powered transition flight [17]. The experimental tests have also been used to create high-fidelity aero-propulsive models using design of experiments (DOE) [18, 19] to develop new system identification techniques specifically for eVTOL aircraft modeling [20–22]. Reference [23] provides a thorough description of the LA-8 testing procedures and discussion on the pitching moment characteristics of the tandem wing aircraft. FlightStream® has previously been validated using the LA-8 forward flight wind tunnel data for both the unpowered and powered airframes [24]. Other related NASA subscale eVTOL aircraft include the GL-10 [13], the predecessor to the LA-8, and the RAVEN-SWFT [15, 16, 25], the successor to the LA-8. Thus far, this experimental series has directly contributed to advancements in high-incidence angle propeller modeling [26–28], aero-propulsive modeling using wind-tunnel testing [13, 20–22, 25, 29, 30], flight controls [31, 32], and flight-test strategies [33, 34] for DEP aircraft.

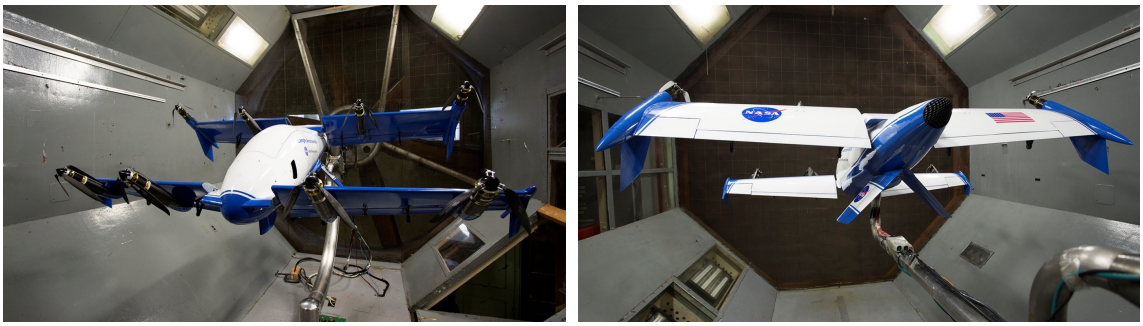
In this paper, an aero-propulsive transition analysis of the LA-8 was conducted using FlightStream® to assess its viability as a preliminary design tool for eVTOL aircraft. This work builds on FlightStream® predictions presented in Ref. [24] by analyzing the transition flight regime, in addition to forward flight conditions. The paper is organized as follows: Section II provides an overview of the LA-8 model geometry. Section III describes the development of the

FlightStream® computational model. Comparisons between FlightStream® solutions and wind tunnel data are given in Sec. IV. Concluding remarks are summarized in Sec V.

II. Model Geometry

The LA-8 is a subscale, tandem tilt-wing aircraft that was developed at NASA Langley as a testbed for eVTOL technology [14, 35]. A photo taken of the LA-8 positioned in the NASA Langley 12-Foot Low-Speed Tunnel is shown in Fig. 1. The LA-8 has two tilting wings, eight electric motors/propellers, four elevons, four flaps, and two ruddervators. An overhead view of the LA-8 is shown in Fig. 2 with labels for each control effector and arrows indicating the rotation direction for each propeller. The propellers are denoted by n, the elevons with δ_e, the flaps with δ_f, and the ruddervator with δ_r. The indices 1 through 4 refer to the front wing control effectors and 5 through 8 refer to the rear wing control effectors. Wing angle is denoted by δ_w with index 1 representing the front wing and index 2 representing the rear wing. Reference geometry for the LA-8 model is given in Table 1.

The publicly available OpenVSP model of the LA-8 was used as the starting geometry for this work [36]. The initial LA-8 OpenVSP model was modified to account for a minor shift of the front wing location and an expansion to the underside of the fuselage. Furthermore, the split where the wings tilt, as seen in Fig. 2, was added to the model.



(a) LA-8 front view. **(b) LA-8 rear view.**

Fig. 1 LA-8 mounted in the NASA Langley 12-Foot Low-Speed Tunnel.

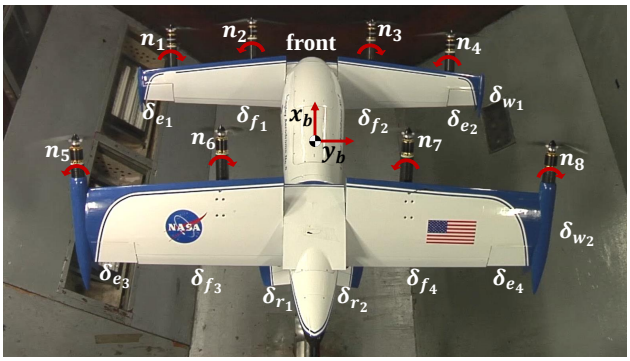
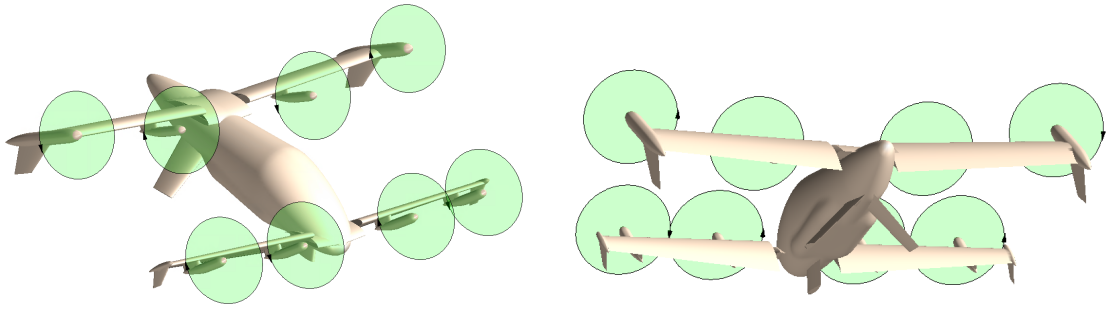


Fig. 2 LA-8 control effector definitions.

Table 1 LA-8 reference geometry [17].

Parameter	Value
front wing span, b_1	5.80 ft
rear wing span, b_2	6.17 ft
reference chord, c_{ref}	0.925 ft
reference area, S_{ref}	11.15 ft^2



(a) LA-8 front view. **(b) LA-8 rear view.**

Fig. 3 LA-8 outer mold line and propeller disks.

Figure 3 shows the resulting outer mold line of the LA-8 used in this work.

III. Computational Model

A. Flow Solver

FlightStream® produces mid-fidelity solutions comparable to RANS CFD at a relatively low computational cost, which makes it ideal for early design [10, 37–39]. FlightStream® is advantageous for both steady and unsteady aerodynamic modeling [12, 40, 41], as modifying and rebuilding a surface mesh is much less demanding than modifying a volumetric mesh. The surface mesh of a given geometry is composed of vortex rings, where the ring segments are the edges of the mesh facets. The surface vorticity is determined by defining a boundary condition at the surface (no-slip, no-normal flow, etc.) that is satisfied by the summation of the induced velocities from the surface vortices according to the Biot-Savart law and freestream conditions. The result is a linear system of equations where the surface vorticity can be determined through inversion. FlightStream® handles inversion issues related to large matrices with a partitioned solver based on a fast-multipole method (FMM) [42]. The surface-vorticity method is inherently a potential formulation since the vorticity is assumed to be contained in an infinitesimal layer on the surface, representing an infinite Reynolds number. FlightStream® builds on the potential flow solution with post-processing models such as laminar, transitional laminar-turbulent, and fully-turbulent boundary layer models, a viscous-coupling model, and surface-based flow separation models. Additionally, compressibility corrections are used for better prediction of higher subsonic flow speeds. Two flow separation models based on Stratford's criterion [43] are available: an axial model and a crossflow model. The axial model is better suited for lifting bodies, whereas the crossflow model is better suited for bluff bodies. Conway actuator disks [44] can be used in FlightStream® to model steady propellers and are used in this work for the powered flight cases. These are steady-state propeller models that take propeller rotational speed and thrust coefficient as inputs. Though not used in this work, unsteady rotor models, or any other geometry motion (including stacked motions), can be modeled in FlightStream® with its unsteady solver. This work uses FlightStream® build 10292023.

B. Mesh Setup

The surface mesh for the LA-8 airframe is shown in Fig. 4. Following a similar process to Ref. [45], the OpenVSP model described previously was exported from OpenVSP as a degenerate geometry (DegenGeom) file, which was then converted into a FlightStream® component cross-section (CCS) file. The CCS file specifies structured mesh parameters, trailing edge designations, and control surface integration, among other parameters, allowing for automatic meshing of the model upon import into FlightStream®. As will be discussed in Sec. III.D, a mesh refinement study was performed to determine an appropriate mesh quality. Two mesh sets were used in this work: a model with full wings for the forward flight conditions and a model with split wings for the transition flight conditions. The cross-section curve generation tool in the FlightStream® CAD creator utility was used to reconstruct the wing surfaces with the split for tilt-wing rotation. The surface mesh was left open at the juncture between the outer wing and inner wing and the wings were rotated about a reference pivot without morphing the mesh. The FlightStream® meshes had approximately 80,000 faces.

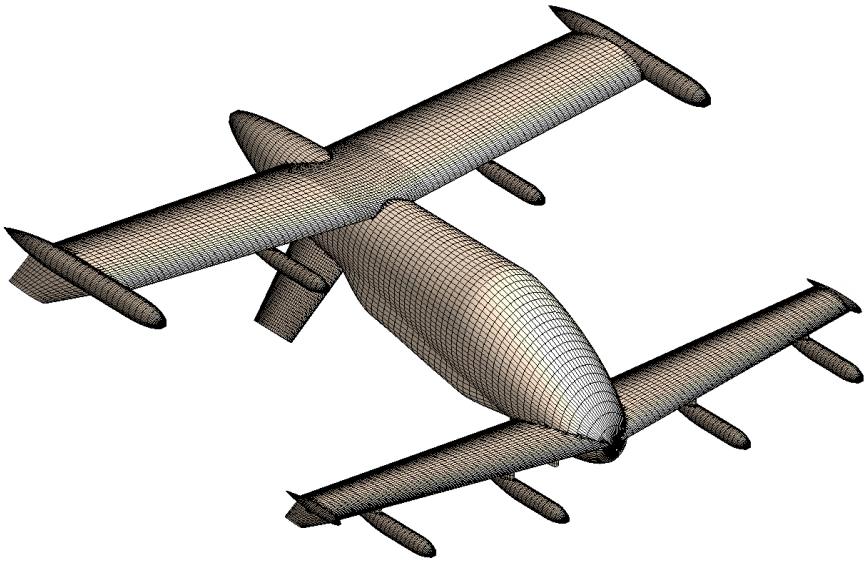


Fig. 4 Surface mesh of the LA-8 model.

C. Solver Settings

All flow simulations considered in this work applied the viscous coupled solver in FlightStream® to the wings. The axial separation model was used on the wings and V-tail, whereas the crossflow separation model was applied to the fuselage. Results are also provided for the inviscid model in which the viscous coupling and flow separation models were removed. Drag predictions are provided using both the pressure and vorticity drag models in FlightStream®. The pressure drag model performs an integration of the predicted surface pressure, which considers the effects of the flow separation model, while the vorticity drag model is based on the Kutta-Joukowski Theroem. The boundary layer was assumed turbulent for all cases because the transitional model is not suited for Reynolds numbers below 5×10^5.

Wake termination nodes are used to prevent a violation of Helmholtz Theorem and are typically needed anywhere a trailing edge terminates into a body, such as at the fuselage. However, placing wake termination nodes where the wingtip trailing edges connect to the wingtip pods was found in preliminary results to lead to an under-prediction in the three-dimensional effects, or in other words, an inaccuracy in the wingtip vortex formation. Consequently, an uncommon physics boundary was imposed at the wing tips where the trailing edges were extended onto the wingtip pods, as shown in Fig. 5. A special physics condition is applied for these trailing-edge extensions to shed shear layer vorticity from the bluff wingtip pods [46]. The majority of the wake strands on these trailing-edge extensions were disabled (shown as the orange dots in Fig. 5) to reduce the relatively high density of wake strands that would result otherwise.

The propellers for the powered cases are modeled with Conway actuator discs [44], which describe the steady operation of a propeller given a thrust coefficient, rotational speed, and disc radius. To determine the thrust output of the

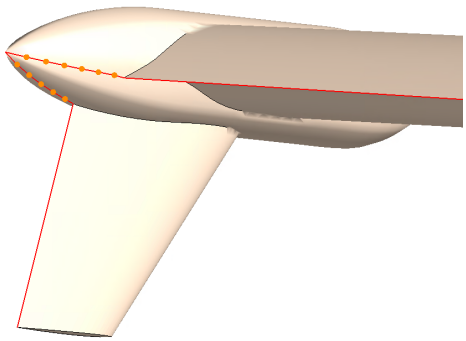


Fig. 5 Special trailing-edge condition at LA-8 wingtips.

propellers at a given RPM and wing angle, an empirical polynomial model [26] is used:

$$C_{T,\text{prop}} = C_{T0} + C_{T1}{J_x}^2 + C_{T2}{J_z}^2 + C_{T3}{Re^*}^3 + C_{T4}{J_x}^3 \tag{1}$$

The model consists of five coefficients and is a function of the normal advance ratio,

$$J_x = \frac{V_\infty}{nD}\cos(i_p) \tag{2}$$

tangential advance ratio,

$$J_z = \frac{V_\infty}{nD}\sin(i_p) \tag{3}$$

and the normalized blade Reynolds number

$$Re^* = \frac{Re - 10^5}{10^5} \tag{4}$$

where the blade Reynolds number is defined as:

$$Re = \frac{0.75\pi\rho n D c_{0.75}}{\mu} \tag{5}$$

The propeller thrust coefficient needs to be converted to the rotor definition for use in FlightStream®. The propeller thrust coefficient definition is

$$C_{T,\text{prop}} = \frac{T}{\rho n^2 D^4} \tag{6}$$

and the rotor thrust coefficient definition is:

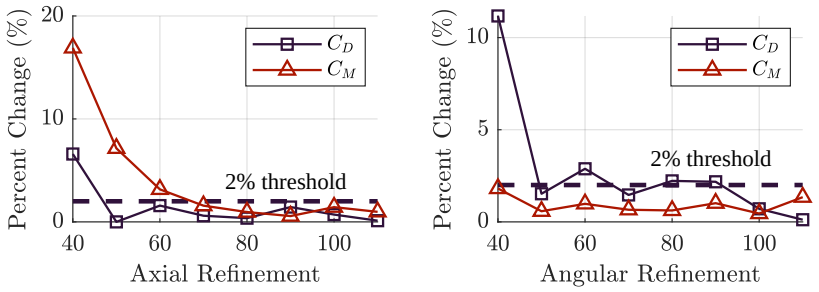
$$C_{T,\text{rotor}} = \frac{T}{\rho\pi R^2(\omega R)^2} = \frac{4}{\pi^3}C_{T,\text{prop}} \tag{7}$$

D. Mesh Refinement Study

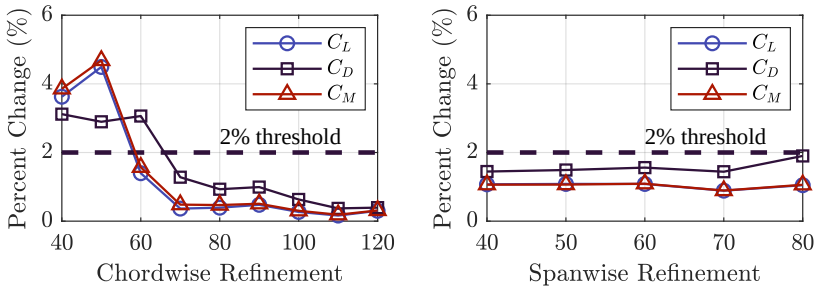
Performing a mesh refinement study is an essential initial step for any analysis using computational aerodynamics software. Specifically, the mesh refinement study identifies potential issues with the model, demonstrates the convergence of individual components of the model, determines an appropriate mesh for the analysis, and instills confidence in the chosen model quality. Generally, for mid-fidelity analyses used in early design stages, only major components need to be considered for the refinement study; for the LA-8, these are the fuselage, rear wing, front wing, and V-tail. Examples of minor components in this investigation that were not included in the refinement study are the endplates of the wings and the pylons of the propellers. Less scrutiny is required for the minor components meshes because they will only have a minor impact on the overall solution. The mesh refinement for the minor components can be chosen to be similar to that of the major components or, to be less conservative and increase computational efficiency, coarser meshing can be applied (within reason).

First, a refinement study is performed in the chordwise/axial direction holding the spanwise/angular refinement constant at a value that will not lead to excessively high aspect ratio elements during the refinement. A suitable chordwise refinement is chosen as the minimum mesh count that satisfies less than 2% change in the dominant loads. The spanwise/angular refinement is then determined by holding the chordwise/axial refinement constant at the value determined from the previous step. The mesh element size should be uniform in both directions; doing so removes additional nonlinear variation in the mesh as the refinement study is performed. The study is most effective if the conditions in the solver are set to a condition that will produce nonzero loads on the model, such as a nonzero angle of attack or sideslip angle. In FlightStream®, it is a best practice to perform the refinement analysis using the inviscid solver.

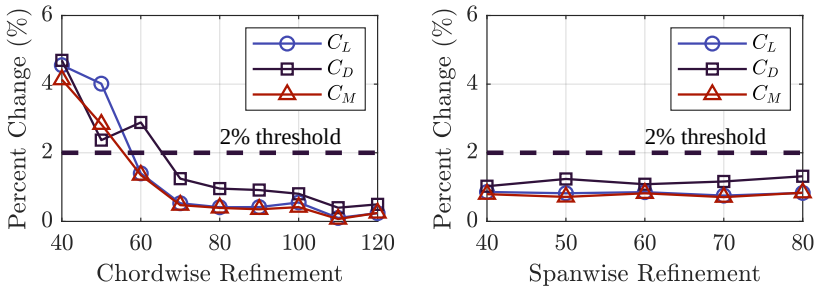
Results for the mesh refinement study of the LA-8 model completed in this work are shown in Fig. 6. The axial or chordwise refinement generally has the most pronounced effect on the loads, as this is the direction that typically has the highest curvature on the geometry. The percent change of the loads drops to the 2% threshold at a fairly coarse mesh refinement and then little to no more improvement is seen as the refinement increases. For example, the rear wing chordwise refinement is seen to surpass the 2% threshold at 70 grid points. The surface-vorticity method is known to be robust to coarse meshes, which is reflected in the results observed. A chordwise refinement of 80 elements was found to be satisfactory for all of the geometry components of interest in this study. The solution is not sensitive to the spanwise refinement of the lifting bodies for the refinement levels used in this analysis.



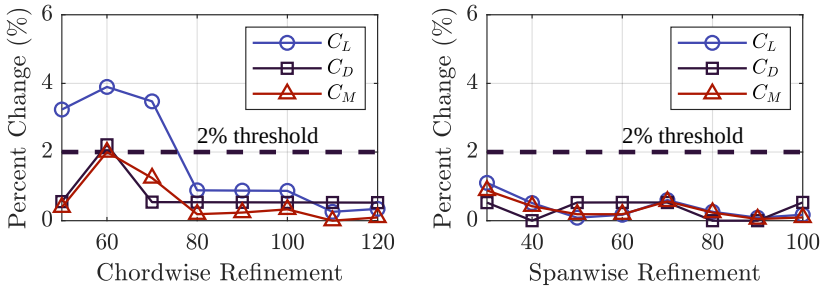
(a) Fuselage refinement



(b) Rear wing refinement



(c) Front wing refinement



(d) V-tail refinement

Fig. 6 Results from the mesh refinement study.

E. Performance and Convergence

A solver convergence tolerance of 10^{-5} based on the stability surface vorticity and wake integration plane was deemed satisfactory for this analysis; the selected convergence tolerance follows the best practices that have been laid out for FlightStream® through other validation studies [38]. Computations were run with 12 parallel processors on a Windows desktop computer. Solutions of the stated convergence were obtained on the order of minutes.

IV. Results and Discussion

Unpowered forward flight and transition analyses are presented in the following subsections. Several powered transition flight conditions are presented as well. Comparisons between FlightStream® and wind tunnel data [17] are provided for lift, drag, and pitching moment coefficients.

Specifically, the experimental data considered from the wind tunnel study can be found in Figures 9, 10, and 11 for the unpowered forward flight and Figures 90, 91, and 93 for the unpowered transition flight in Ref. [17]. The powered results are compared to the LA-8 aero-propulsive model documented in Ref. [21] that was developed using data from several wind tunnel tests [21, 23]; the bounds for the case with a dynamic pressure of 3.5 psf are provided in Table 2. Several flight conditions were run in FlightStream® within these bounds for the powered cases.

Table 2 Aero-propulsive model domain for $\bar{q}$ = 3.5 psf.

Parameter	Domain
angle of attack, α (deg)	[-6 , 6]
sideslip angle, β (deg)	[-5 , 5]
wing angle, δ_w (deg)	[0 , 25]
elevon deflection, δ_e (deg)	[-25 , 25]
propeller speed, n (RPM)	[1900 , 6500]

The control effectors are undeflected for all cases considered in this investigation. The following abbreviations are used to present the results: WT for wind tunnel data, RSE for wind-tunnel-derived response surface equation, and FS for FlightStream®. The FlightStream® results are labeled with two subscripts: the first subscript denotes the viscous solver type, with v indicating the viscous coupling and flow separation models are enabled and i indicating that only the the inviscid solver is applied; the second subscript indicates the drag model used, with P representing the pressure drag model and V representing the vorticity drag model.

A. Isolated Airframe Forward Flight

Unpowered forward flight analyses data were collected over a range of angles of attack at a dynamic pressure setting of 2.1 psf. The results are shown in Fig. 7 with comparisons made to the wind tunnel data [17].

In the wind tunnel lift data, two peaks are observed at approximately 15 and 25 degrees. These correspond to the initial 'soft stall' of the front wing, followed by the stall of the rear wing. Despite FlightStream® not capturing this soft stall very well, the solver predicts the overall lift trend well up to the first stall. The slope of the lift curve for the inviscid solver is similar to the slope of the linear region of the experimental data. A slight offset in magnitude of the

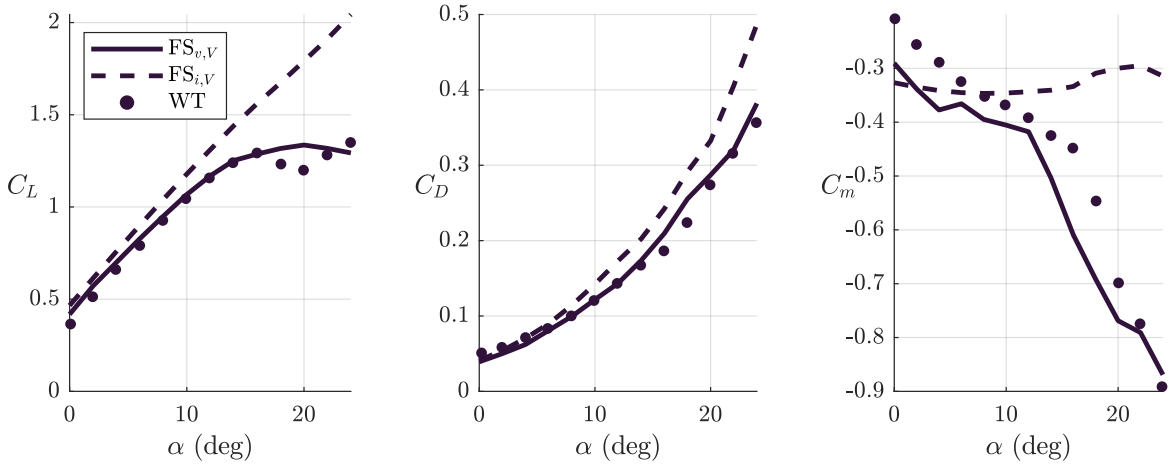


Fig. 7 Unpowered forward flight of the LA-8 with $\bar{q}$ = 2.1 psf.

inviscid solution is observed compared to the viscous-coupled solution at the lower angles of attack, and slightly more so compared to the experimental data. This indicates that substantial viscous effects are occurring at the lower angles of attack. A possible cause of this is the shape of the fuselage, particularly the up-swept underside; this likely encourages flow separation on the fuselage underside at the lower angles of attack. The drag predictions from FlightStream® agree well with the experimental data. The reduction in lift due to the viscous-coupling losses leads to a reduction in the induced drag, which improves on the overprediction in drag observed with the inviscid solver. At zero angle of attack, the drag prediction begins to diverge from the experimental data, again, most likely due to the severity of flow separation under the fuselage at these angles. The pitching moment prediction from FlightStream® follows the expected trend observed from the experimental study. The impact of the viscous-coupling and flow separation models is most noticeable when comparing the difference between the inviscid and viscous pitching moment results. The inviscid solver moment prediction is only similar in magnitude around 8 degrees, and the slope does not follow any part of the experimental curve. The slope from the viscous solver follows the experimental data over the entire range investigated.

B. Unpowered Transition Flight

In this section, results for the bare-airframe transition analysis are presented. Lift, drag, and pitching moment coefficients are provided for various wing angles. The LA-8 model with split wings is used in this analysis, as well as in the following powered transition analysis that will be presented in Sec. IV.C, to allow rotation of the outer wing sections. The results are compared with experimental wind-tunnel data [17]. The plots show the wind tunnel data compared to the inviscid and viscous FlightStream® solutions.

The unpowered transition flight results are presented in Fig. 8. The dynamic pressure is 2.1 psf and the angle of attack is set to 2 degrees. The wind-tunnel-derived lift is predicted reasonably well by FlightStream®, however, the peak lift at approximately 18 degrees is under-predicted. This is possibly an over-prediction in flow separation by the separation model. Considering this under-prediction was not observed in the forward flight case, this discrepancy is presumably caused by the junction where the tilting wings rotate. After stall, FlightStream® accurately predicts the drop in lift but begins to diverge from the experimental data around a wing angle of 32 degrees.

Drag results are presented for both the vorticity drag model and the pressure drag model. The vorticity drag model follows the experimental data well up to 32 degrees, and for higher wing angles the model overpredicts drag. The pressure drag model for the viscous solution has more accurate drag predictions in magnitude for the high wing angles, but underpredicts the drag below for wing angles between 20 and 40 degrees.

The peak pitching moment is underpredicted by FlightStream®. Prior to and just after this peak, FlightStream® predicts the pitching moment fairly well. The moment begins to diverge from the experimental data above 30-degree

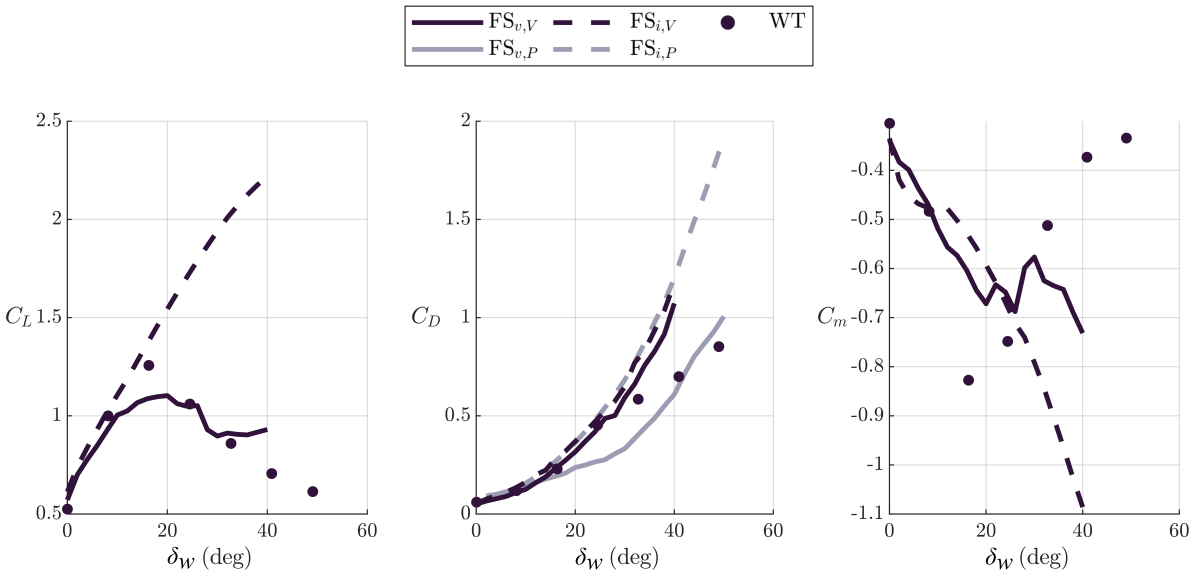


Fig. 8 Unpowered transition analysis for the LA-8 at α = 2 deg and $\bar{q}$ = 2.1 psf.

wing angle. The viscous solution follows the experimental trend slightly better than the inviscid solution for wing angles between 0 and 20 degrees. The inviscid solution's slope is always negative, while the viscous solution changes sign similar to the wind tunnel trend.

C. Powered Transition Flight

Results for the powered transition analysis are provided for various wing angles. The results were compared to response surface equations constructed from statistically designed wind-tunnel experiments [21]. The powered cases are trimmed at each stage of transition investigated. To do so, the aero-propulsive model was first used to determine the thrust required at a given wing angle to balance the weight and drag of the aircraft, where the thrust of each of the eight propellers was set to be equal. Then, the thrust difference between the front wing and rear wing propellers was set (while maintaining the same net thrust found previously) to balance the pitching moment. The wing angles at each stage of the transition flight envelope were chosen to be the same as those used in the experimental work [17]. Six trimmed conditions, shown in Table 3, corresponding to different stages in the transition flight of the LA-8 are explored for this aero-propulsive analysis. The state and control variables for each condition are set to values that the LA-8 experiences during its transition; high dynamic pressure settings correspond to low wing angles and the wing angle increases as the dynamic pressure setting decreases. All other control surfaces are held at their neutral setting. The LA-8 isolated propeller model [26] is used to determine the appropriate thrust coefficient given the wing/propeller incidence, dynamic pressure, and propeller rotational speed. The determined thrust coefficients that were used in FlightStream® for each case are given in Table 4. The thrust coefficient for a given rotational speed setting is slightly higher for the clockwise rotating propeller as compared to the counterclockwise rotating propeller. This is a result of manufacturing differences between the clockwise and counterclockwise propellers [27]. This physical asymmetry is incorporated into the FlightStream® analysis to provide a direct comparison to the wind tunnel data.

Results for the cases with low and high wing angles are shown in Fig. 9 and Fig. 10, respectively. The pressure drag model was found to be more accurate for both magnitude and slope than the vorticity drag model for all cases considered; as such, the case presented in Fig. 9 and Fig. 10 used the pressure drag model. Figure 12 in Appendix A shows a comparison of the two drag models for these powered cases.

As seen in Fig. 9, FlightStream® has good agreement with the lift and drag for the low wing angle cases, particularly

Table 3 Trimmed conditions for the powered transition cases.

$\bar{q}$	δ_{w_1}	δ_{w_2}	$n_1,\ n_2,\ n_3,\ n_4$	$n_5,\ n_6,\ n_7, n_8$
psf	deg	deg	RPM	RPM
5	0	0	5360	4680
4.5	12	9	4790	4360
2.5	30	22	4470	4060
1.5	42	42	4850	4400
1	51	51	5140	4780
0.5	63	63	5440	5340

Table 4 Thrust coefficients at each trim condition.

$\bar{q}$ (psf)	C_{T_1}	C_{T_2}	C_{T_3}	C_{T_4}	C_{T_5}	C_{T_6}	C_{T_7}	C_{T_8}
5	0.0063	0.0054	0.0063	0.0054	0.0026	0.0036	0.0026	0.0036
4.5	0.0055	0.0046	0.0055	0.0046	0.0024	0.0035	0.0024	0.0035
2.5	0.0102	0.0090	0.0102	0.0090	0.0070	0.0083	0.0070	0.0083
1.5	0.0134	0.0117	0.0134	0.0117	0.0113	0.0130	0.0113	0.0130
1	0.0147	0.0124	0.0147	0.0124	0.0123	0.0145	0.0123	0.0145
0.5	0.0154	0.0128	0.0154	0.0128	0.0128	0.0154	0.0128	0.0154

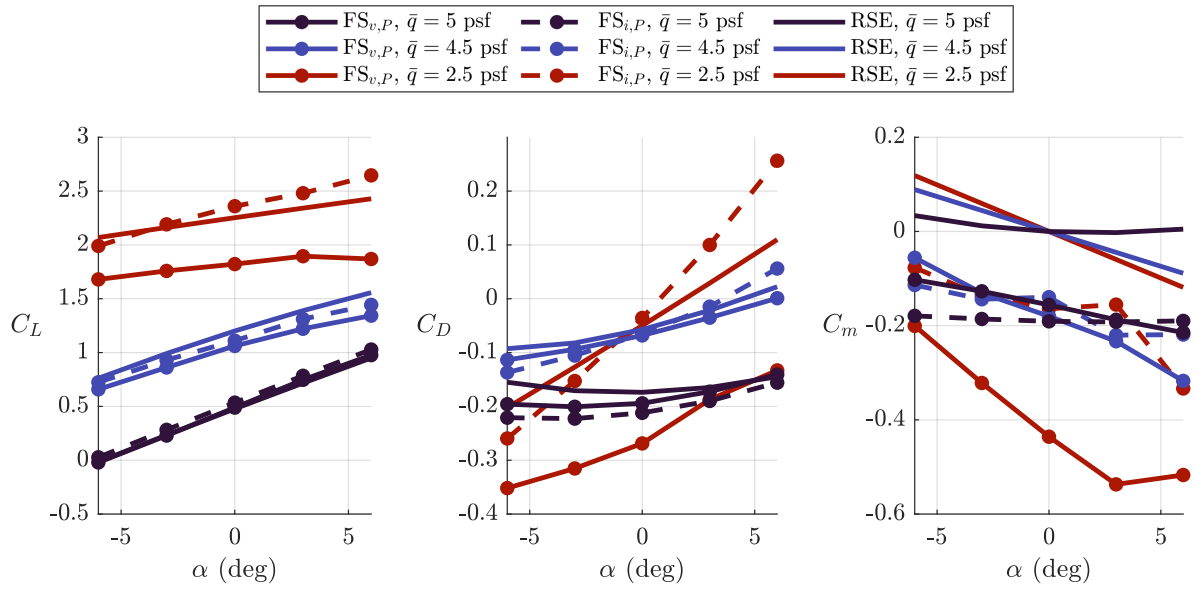


Fig. 9 Powered low wing angle transition analysis results for the LA-8.

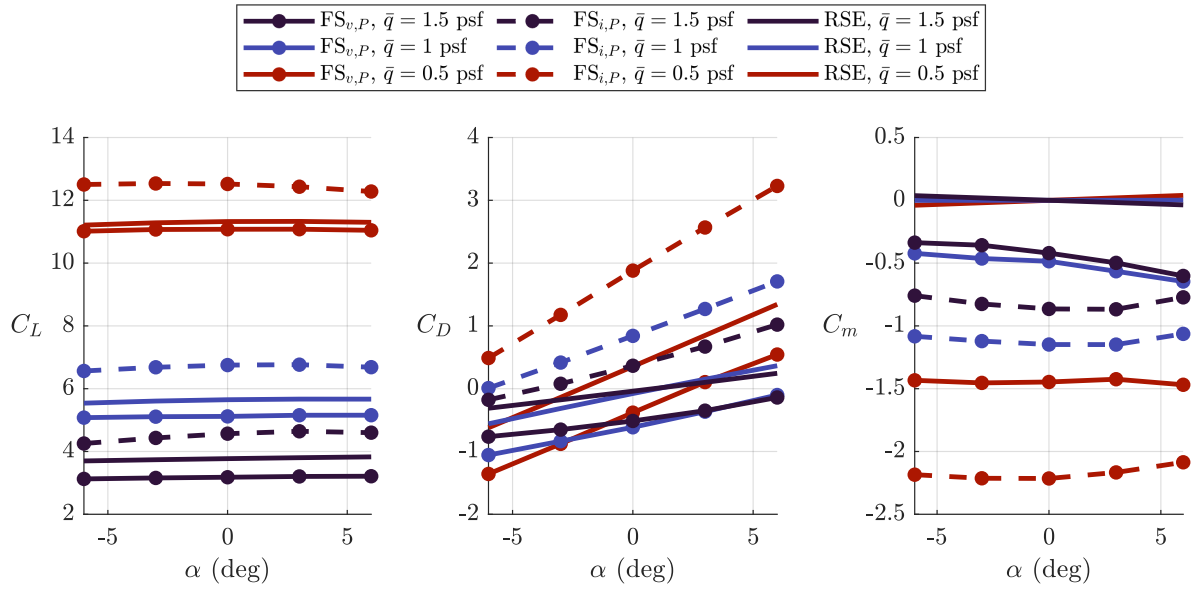


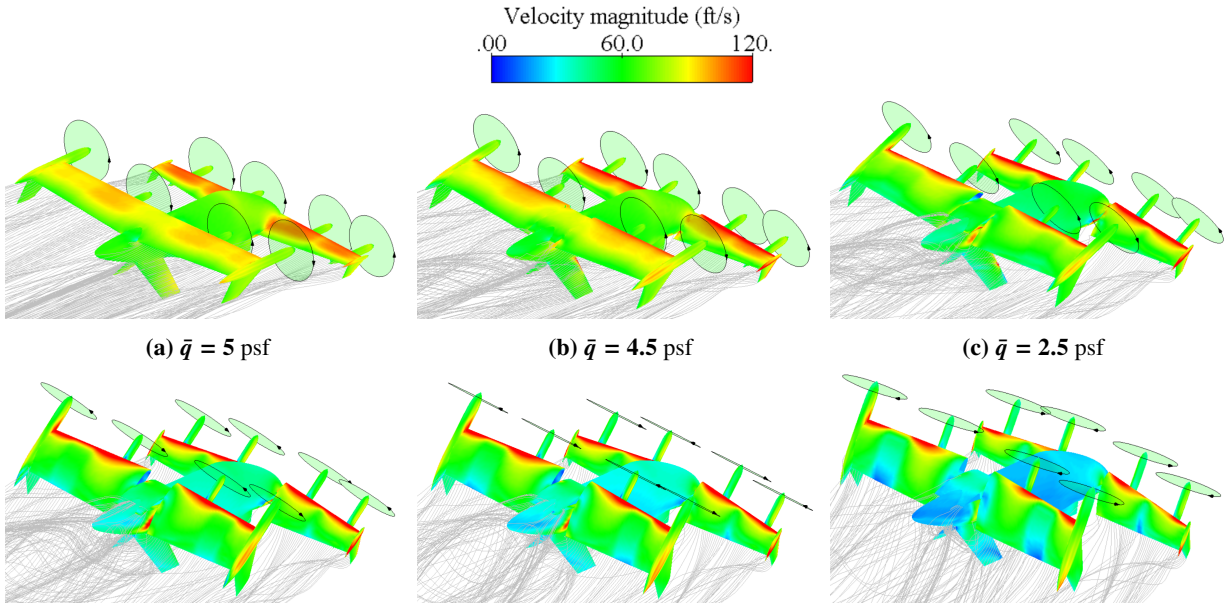
Fig. 10 Powered high wing angle transition analysis results for the LA-8.

for $\bar{q}$ = 5 psf and $\bar{q}$ = 4.5 psf. At $\bar{q}$ = 2.5 psf, the viscous results underpredict the lift and drag substantially, likely attributed to overprediction from the flow separation model. The inviscid lift and drag results for the $\bar{q}$ = 2.5 psf case are closer to the RSE results, however, the slope deviates more from the trend of the RSE as compared to the lower wing angle cases. The pitching moments from FlightStream® are offset from the RSE results for all the low wing angle cases considered, although, the slopes are similar.

Similar to the $\bar{q}$ = 2.5 psf case from Fig. 9, significant differences are observed in the lift prediction for $\bar{q}$ = 1.5 psf and $\bar{q}$ = 1 psf in the mid transition regime shown in Fig. 10. Despite the offset, the lift slope follows the RSE trend well. The RSE lift is bounded by the inviscid and viscous FlightStream® results, indicating an over-correction by the viscous models. For the highest wing angle tested, at $\bar{q}$ = 0.5, the FlightStream® viscous model lift prediction is much closer to the RSE lift. The drag predictions from the viscous solver have similar slopes to the RSE results for all the high wing angle cases, although, there is an offset between FlightStream® predictions and the RSE. This can likely be attributed

to an overprediction in thrust for the propeller models because the thrust coefficient predictions are for the isolated propeller and do no include integration losses. As has been seen for the low wing angle cases, the moment prediction from FlightStream® has considerable differences in magnitude compared to the RSE moment results, with the worst error seen for the case of $\bar{q} = 0.5$ psf.

Velocity contours for the investigated powered LA-8 transition flight conditions are presented in Fig. 11 with an angle of attack of 6 degrees. As the wings transition to hover, the freestream velocity decreases, as can be inferred by the velocity magnitude seen on the fuselage. The effect of the induced flow from the propellers can be observed on the front and rear wings. At high wing angles, a stalled flow region is observed between the two wakes of the propellers on either side, both on the front and rear wings. The wingtip pods show a relatively high velocity on the outer sides of the pods near the trailing edge, which is caused by the shedding of wingtip vortices and induced flow of the outer propellers. The wing tip trailing edge condition discussed in Sec. III.C allows the effect of flow separation between the outer and inner sides of the wing tip pods to be modeled.



(a) $\bar{q}$ **= 5** psf **(b)** $\bar{q}$ **= 4.5** psf **(c)** $\bar{q}$ **= 2.5** psf

(d) $\bar{q}$ **= 1.5** psf **(e)** $\bar{q}$ **= 1** psf **(f)** $\bar{q}$ **= 0.5** psf

Fig. 11 Velocity contours from the powered transition analysis at an α **=** 6 **deg.**

V. Concluding Remarks

An aero-propulsive analysis of the LA-8 in transition flight was performed using the FlightStream® surface-vorticity solver, a mid-fidelity aerodynamic prediction tool suited for early design stages. Results were presented for the isolated, unpowered airframe in forward flight and transition flight, and powered transition flight using Conway actuator discs.

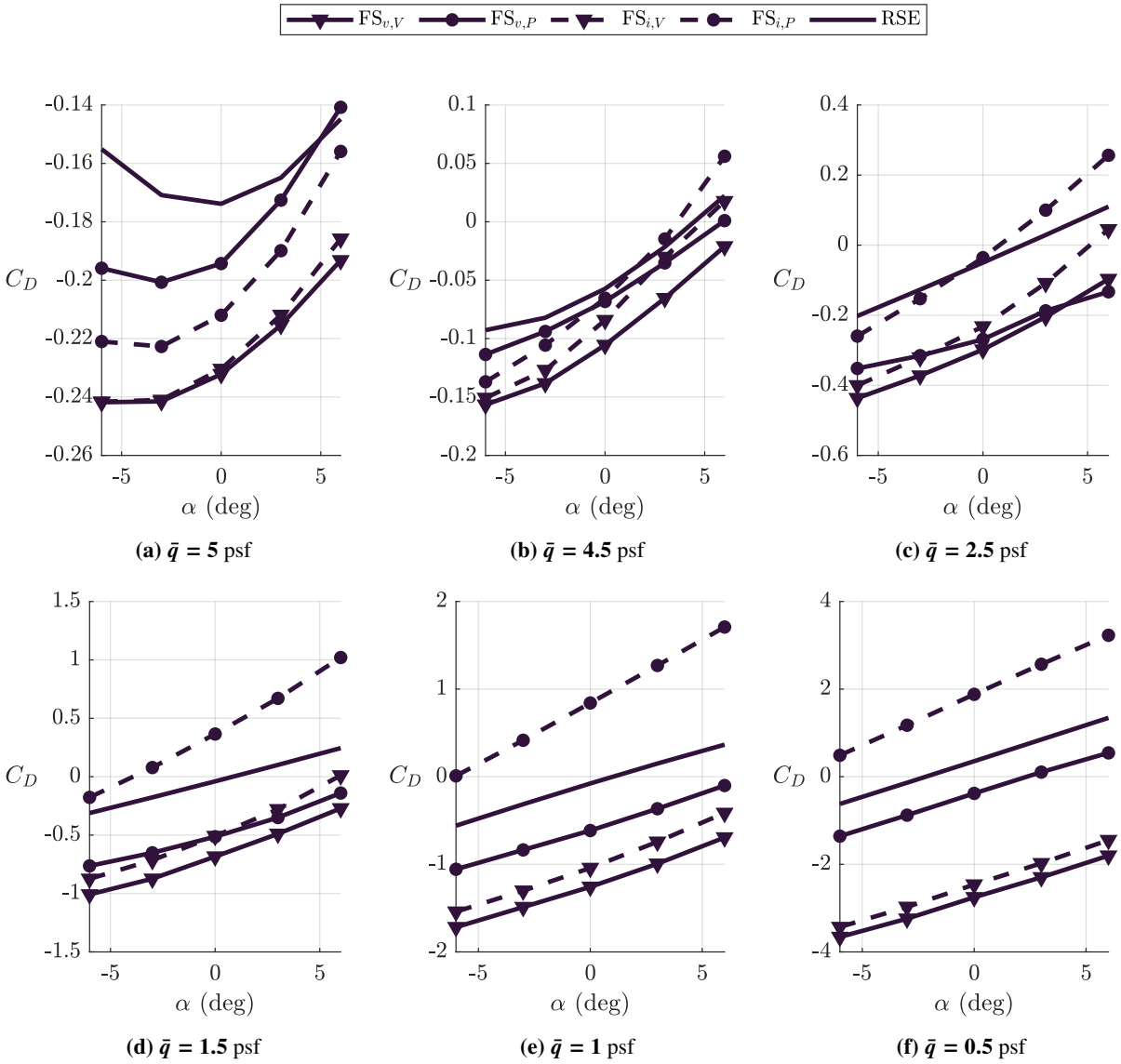
For the unpowered forward flight case, FlightStream® had good agreement with the experimental data for lift, drag, and pitching moment for the angle of attack range investigated. For the unpowered transition flight, FlightStream®'s lift and pitching moment predictions followed the experimental trends until approximately an angle of attack of 32 degrees, where the predictions begin to diverge. The peak lift and pitching moment observed in the experimental data near an angle of attack of 18 degrees was underpredicted by FlightStream®, most likely due to modeling deficiencies with the flow separation model near the tilt-wing junction. The FlightStream® drag predictions also begin to diverge from the experimental data near an angle of attack of 32 degrees using the vorticity drag model. However, the pressure drag model performed much better for the high wing angle cases because this model takes into account the flow separation effects whereas the vorticity drag model does not.

For the powered transition flight, analyses were conducted at trim conditions determined with the aero-propulsive model [21] at different dynamic pressure settings. The pressure drag model was found to yield better predictions as compared to the vorticity drag model for all the powered cases considered. FlightStream® had reasonably accurate

lift and drag predictions for the high speed transition cases w ith more differences between the wind tunnel data and FlightStream® predictions seen in pitching moment. FlightStream® solutions had the most error in the lift and drag predictions for the mid-transition regime. For the majority of these transition cases, the lift and drag slopes were predicted reasonably well by FlightStream® with an offset from the RSE result. The drag difference is partially attributed to an overprediction in thrust, because the thrust of the propellers is determined from a model developed for the propellers in isolation. Furthermore, the flow separation model does not take into account the induced flow from the propellers, which likely also contributes to the error. If a true data point is known, such as the known performance of a trimmed flight condition during transition, the data from FlightStream® can be offset with respect to this known performance and the lift and drag slopes from FlightStream® used to make accurate predictions.

FlightStream® has been shown to be useful tool for conducting transition aero-propulsive analyses of eVTOL aircraft in early design stages, whereby medium fidelity solutions can be obtained in a time-effective manner. The viscous models accurately capture effects up to and slightly beyond initial stall angles. The solver tends to struggle at capturing the bluff body separation effects, such as cases with high wing angles or angles of attack.

Appendix A: Comparison of Drag Models in Powered Transition



(a) $\bar{q}$ = 5 psf **(b) $\bar{q}$ = 4.5** psf **(c) $\bar{q}$ = 2.5** psf

(d) $\bar{q}$ = 1.5 psf **(e) $\bar{q}$ = 1** psf **(f) $\bar{q}$ = 0.5** psf

Fig. 12 Comparison between the vorticity, pressure drag models, and RSE for the powered transition flight cases.

Acknowledgments

This research was funded by the NASA Aeronautics Research Mission Directorate (ARMD) Transformational Tools and Technologies (TTT) project. Most of this work was conducted under the NASA Office of STEM Engagement (OSTEM) Internship Program, with funding provided by the TTT project.

References

[1] Saeed, A. S., Younes, A. B., Cai, C., and Cai, G., "A Survey of Hybrid Unmanned Aerial Vehicles," *Progress in Aerospace Sciences*, Vol. 98, 2018, pp. 91–105. https://doi.org/10.1016/j.paerosci.2018.03.007.

[2] Johnson, W., and Silva, C., "NASA Concept Vehicles and the Engineering of Advanced Air Mobility Aircraft," *The Aeronautical Journal*, Vol. 126, No. 1295, 2022, pp. 59–91. https://doi.org/10.1017/aer.2021.92.

[3] Kim, H. D., Perry, A. T., and Ansell, P. J., "A Review of Distributed Electric Propulsion Concepts for Air Vehicle Technology," *2018 AIAA/IEEE Electric Aircraft Technologies Symposium*, AIAA Paper 2018-4998, 2018. https://doi.org/10.2514/6.2018-4998.

[4] Silva, C., Johnson, W. R., Solis, E., Patterson, M. D., and Antcliff, K. R., "VTOL Urban Air Mobility Concept Vehicles for Technology Development," *2018 Aviation Technology, Integration, and Operations Conference*, AIAA Paper 2018-3847, 2018. https://doi.org/10.2514/6.2018-3847.

[5] Vempati, L., Geffard, M. V., and Anderegg, A., "Challenges and Decisions for Near-term Integration of Urban Air Mobility (UAM) Operations," *AIAA AVIATION 2022 Forum*, AIAA Paper 2022-3402, 2022. https://doi.org/10.2514/6.2022-3402.

[6] Palaia, G., Abu Salem, K., Cipolla, V., Binante, V., and Zanetti, D., "A Conceptual Design Methodology for e-VTOL Aircraft for Urban Air Mobility," *Applied Sciences*, Vol. 11, No. 22: 10815, 2021. https://doi.org/10.3390/app112210815.

[7] Chakraborty, I., and Mishra, A. A., "Sizing and Analysis of a Lift-Plus-Cruise VTOL Aircraft with Electrified Propulsion Systems," *AIAA AVIATION 2022 Forum*, AIAA Paper 2022-3513, 2022. https://doi.org/10.2514/6.2022-3513.

[8] Slotnick, J., Khodadoust, A., Alonso, J., Darmofal, D., Gropp, W., Lurie, E., and Mavriplis, D., "CFD Vision 2030 Study: A Path to Revolutionary Computational Aerosciences," NASA CR–2014-218178, 2014.

[9] Ahuja, V., Hartfield, R. J., and Ciliberti, D., "Three-dimensional Viscous Coupling & Flow Separation Enhancements to an Inviscid Surface Vorticity Flow Solver," *AIAA SCITECH 2023 Forum*, AIAA Paper 2023-2455, 2023. https://doi.org/10.2514/6.2023-2455.

[10] Ahuja, V., and Hartfield, R. J., "Aerodynamic Loads over Arbitrary Bodies by Method of Integrated Circulation," *Journal of Aircraft*, Vol. 53, No. 6, 2016, pp. 1719–1730. https://doi.org/10.2514/1.C033619.

[11] Zhang, Y., Ahuja, V., Hartfield, R., and Verstraete, D., "Mid-Fidelity Numerical calculation of XV-15 Proprotor," *AIAA SCITECH 2024 Forum*, 2024. https://doi.org/10.2514/6.2024-1509.

[12] Ahuja, V., and Litherland, B. L., "Comparison of Aerodynamic Analysis Tools Applied to a Propeller-Blown Wing," *AIAA SCITECH 2023 Forum*, AIAA Paper 2023-1753, 2023. https://doi.org/10.2514/6.2023-1753.

[13] Rothhaar, P. M., Murphy, P. C., Bacon, B. J., Gregory, I. M., Grauer, J. A., Busan, R. C., and Croom, M. A., "NASA Langley Distributed Propulsion VTOL TiltWing Aircraft Testing, Modeling, Simulation, Control, and Flight Test Development," *14th AIAA Aviation Technology, Integration, and Operations Conference*, AIAA Paper 2014-2999, 2014. https://doi.org/10.2514/6.2014-2999.

[14] North, D. D., Busan, R. C., and Howland, G., "Design and Fabrication of the LA-8 Distributed Electric Propulsion VTOL Testbed," *AIAA SciTech 2021 Forum*, AIAA Paper 2021-1188, 2021. https://doi.org/10.2514/6.2021-1188.

[15] Geuther, S. C., Simmons, B. M., and Ackerman, K. A., "Overview of the Subscale RAVEN Flight Controls and Modeling Testbed," *Vertical Flight Society's 80th Annual Forum & Technology Display*, May 2024.

[16] German, B., Jha, A., Welstead, J., Whiteside, S., and Blaesser, N. J., "Design and Programmatic Overview of the Research Aircraft for eVTOL Enabling techNologies (RAVEN) Activity," *AIAA AVIATION 2023 Forum*, AIAA Paper 2023-3924, 2023. https://doi.org/10.2514/6.2023-3924.

[17] Geuther, S. C., North, D. D., and Busan, R. C., "Investigation of a Tandem Tilt-wing VTOL Aircraft in the NASA Langley 12-Foot Low-Speed Tunnel," NASA TM–20205003178, Jun. 2020.

[18] Montgomery, D. C., *Design And Analysis of Experiments*, 8th ed., John Wiley & Sons, Inc., Hoboken, NJ, 2013.

[19] Myers, R. H., Montgomery, D. C., and Anderson-Cook, C. M., *Response Surface Methodology: Process and Product Optimization Using Designed Experiments*, 4th ed., John Wiley & Sons, 2016.

[20] Simmons, B. M., Morelli, E. A., Busan, R. C., Hatke, D. B., and O'Neal, A. W., "Aero-Propulsive Modeling for eVTOL Aircraft Using Wind Tunnel Testing with Multisine Inputs," *AIAA AVIATION 2022 Forum*, AIAA Paper 2022-3603, 2022. https://doi.org/10.2514/6.2022-3603.

[21] Simmons, B. M., and Murphy, P. C., "Aero-Propulsive Modeling for Tilt-Wing, Distributed Propulsion Aircraft Using Wind Tunnel Data," *Journal of Aircraft*, Vol. 59, No. 5, 2022, pp. 1162–1178. https://doi.org/10.2514/1.C036351.

[22] Simmons, B. M., "Evaluation of Response Surface Experiment Designs for Distributed Propulsion Aircraft Aero-Propulsive Modeling," *AIAA SCITECH 2023 Forum*, AIAA Paper 2023-2251, 2023. https://doi.org/10.2514/6.2023-2251.

[23] Busan, R. C., Murphy, P. C., Hatke, D. B., and Simmons, B. M., "Wind Tunnel Testing Techniques for a Tandem Tilt-Wing, Distributed Electric Propulsion VTOL Aircraft," *AIAA SciTech 2021 Forum*, AIAA Paper 2021-1189, 2021. https://doi.org/10.2514/6.2021-1189.

[24] Geuther, S., and Fei, X., "LA-8 Computational Analysis and Validation Studies Using FlightStream," *AIAA SciTech 2021 Forum*, AIAA Paper 2021-1191, 2021. https://doi.org/10.2514/6.2021-1191.

[25] Simmons, B. M., and Busan, R. C., "Statistical Wind-Tunnel Experimentation Advancements for eVTOL Aircraft Aero-Propulsive Model Development," *AIAA SCITECH 2024 Forum*, AIAA Paper 2024-2482, 2024. https://doi.org/10.2514/6.2024-2482.

[26] Simmons, B. M., "System Identification for Propellers at High Incidence Angles," *Journal of Aircraft*, Vol. 58, No. 6, 2021, pp. 1336–1350. https://doi.org/10.2514/1.C036329.

[27] Simmons, B. M., and Hatke, D. B., "Investigation of High Incidence Angle Propeller Aerodynamics for Subscale eVTOL Aircraft," NASA TM–20210014010, 2021.

[28] Stratton, M., and Landman, D., "Wind Tunnel Test and Empirical Modeling of Tilt-Rotor Performance for EVTOL Applications," *AIAA SciTech 2021 Forum*, AIAA Paper 2021-0834, 2021.

[29] Busan, R. C., Rothhaar, P. M., Croom, M. A., Murphy, P. C., Grafton, S. B., and O'Neal, A. W., "Enabling Advanced Wind-Tunnel Research Methods Using the NASA Langley 12-Foot Low Speed Tunnel," *14th AIAA Aviation Technology, Integration, and Operations Conference*, AIAA Paper 2014-3000, 2014. https://doi.org/10.2514/6.2014-3000.

[30] Murphy, P. C., and Landman, D., "Experiment Design for Complex VTOL Aircraft with Distributed Propulsion and Tilt Wing," *AIAA Atmospheric Flight Mechanics Conference*, AIAA Paper 2015-0017, 2015. https://doi.org/10.2514/6.2015-0017.

[31] Cooper, J. R., Ackerman, K. A., Rothhaar, P. M., and Gregory, I. M., "Autonomous Path-Following for a Tilt_wing, Distributed Electric Propulsion, Vertical Take-Off and Landing Unmanned Aerial System in Hover Mode," NASA TM–2018220109, 2018.

[32] Cook, J., and Gregory, I., "A Robust Uniform Control Approach for VTOL Aircraft," *VFS Autonomous VTOL Technical Meeting and Electric VTOL Symposium*, 2021.

[33] McSwain, R. G., Glaab, L. J., and Theodore, C. R., "Greased Lightning (GL-10) Performance Flight Research – Flight Data Report," NASA TM–2017219794, 2017.

[34] Fredericks, W. J., McSwain, R. G., Beaton, B. F., Klassman, D. W., and Theodore, C. R., "Greased Lightning (GL-10) Flight Testing Campaign," NASA TM–2017219643, 2017.

[35] McSwain, R. G., Geuther, S. C., Howland, G., Patterson, M. D., Whiteside, S. K., and North, D. D., "An Experimental Approach to a Rapid Propulsion and Aeronautics Concepts Testbed," NASA TM–2020-220437, 2020.

[36] Cody, S., "LA-8 Initial Conceptual Design," https://airshow.openvsp.org/vsp/9tFgVhmsVbn4B8V38oCL, Accessed 17 November 2024.

[37] Ahuja, V., Chakraborty, I., and Hartfield, R. J., "Aero-Propulsive Analysis for Contemporary Conceptual Design," *AIAA Aviation 2019 Forum*, AIAA Paper 2019-3019, 2019. https://doi.org/10.2514/6.2019-3019.

[38] DiMaggio, G. A., Hartfield, R. J., and Ahuja, V., "Rapid Prediction of Hybrid Wing Body Aerodynamics," *AIAA AVIATION 2022 Forum*, AIAA Paper 2022-3298, 2022. https://doi.org/10.2514/6.2022-3298.

[39] DiMaggio, G. A., Hartfield, R. J., and Ahuja, V., "Hybrid Wing Body Pitch Control with a Surface-Vorticity Solver," *AIAA SCITECH 2023 Forum*, AIAA Paper 2023-0623, 2023. https://doi.org/10.2514/6.2023-0623.

[40] Pastor, G., Hartfield, R., and Ahuja, V., "Expedited Solutions for Propeller Analysis," *AIAA SCITECH 2022 Forum*, AIAA Paper 2022-1158, 2022. https://doi.org/10.2514/6.2022-1158.

[41] Brown, G. E., and Ahuja, V., "The Stopped Rotor Concept – A New Look At An Old Idea," *AIAA AVIATION 2023 Forum*, AIAA Paper 2023-4388, 2023. https://doi.org/10.2514/6.2023-4388.

[42] Ahuja, V., and Hartfield, R. J., "Aerodynamic Loads over Arbitrary Bodies by Method of Integrated Circulation," Ph.D. Dissertation, Dept. of Aerospace Engineering., Auburn University, Auburn, AL, 2013. URL https://arc.aiaa.org/doi/10.2514/1.C033619.

[43] Stratford, B. S., "The prediction of separation of the turbulent boundary layer," *Journal of Fluid Mechanics*, Vol. 5, No. 1, 1959, p. 1–16. https://doi.org/10.1017/S0022112059000015.

[44] Conway, J. T., "Analytical solutions for the actuator disk with variable radial distribution of load," *Journal of Fluid Mechanics*, Vol. 297, 1995, p. 327–355. https://doi.org/10.1017/S0022112095003120.

[45] Simmons, B. M., Geuther, S., and Ahuja, V., "Validation of a Mid-Fidelity Approach for Aircraft Stability and Control Characterization," *AIAA AVIATION 2023 Forum*, AIAA Paper 2023-4076, 2023. https://doi.org/10.2514/6.2023-4076.

[46] Katz, J., and Plotkin, A., *Low-Speed Aerodynamics*, 2nd ed., Cambridge Aerospace Series, Cambridge University Press, 2001.